Adsorption and Depletion of Polyelectrolytes in Charged Cylindrical System within Self-Consistent Field Theory

Xingkun Man,[†] Shuang Yang,[†] Dadong Yan,*[,†] and An-Chang Shi[‡]

Beijing National Laboratory Molecular Sciences (BNLMS), Joint Laboratory of Polymer Science and Materials, Institute of Chemistry, Chinese Academy of Sciences, Beijing 100080, China, and Department of Physics and Astronomy, McMaster University, Hamilton, Ontario L8S 4M1, Canada

Received February 17, 2008; Revised Manuscript Received May 14, 2008

ABSTRACT: Self-consistent field theory (SCFT) is presented to study the adsorption of flexible polyelectrolytes (PE) onto uniformly oppositely charged cylinders. We focus on the curvature effect of adsorbing surface on the adsorption−depletion phase-transition-like behavior. Numerical solutions for SCFT functions are derived. In terms of the scaling expression ($C^*_{salt} \sim p^{\alpha}\sigma^{\beta}$) of the critical quantities, i.e., the salt concentration C^*_{salt}, the charge fraction p of PE chain and the area density of surface charge σ, at the adsorption−depletion transition point, we divide the whole curvature dimension into two regimes, i.e., the planar regime and the cylindrical regime. In particular, we have numerically determined the crossover point of the two regimes at which the cylinder radius r_0 approximately equates to 2 times the gyration radius R_g of PE chain, or, $r_0 \sim 2R_g$. In the planar regime ($r_0 > 2R_g$), the scaling expression is invariable with surface curvature and is reduced to the planar case, or $C^*_{salt} \sim (p\sigma)^{2/3}$. In the cylindrical regime ($r_0 < 2R_g$), the exponents in the scaling expression increase as r_0 decreases and lead to $C^*_{salt} \sim p^{0.78}\sigma^{0.86}$ for a large surface curvature $r_0 = 0.1R_g$. Moreover, we find a critical line for the dependence of the critical radius of cylinder on the salt concentration, which separates the adsorption and depletion states. The theoretical results are in good agreement with the Monte Carlo simulations and the experimental results.

I. Introduction

The adsorption of polyelectrolytes (PE) onto charged surfaces is always relevant to biological systems and has numerous industrial applications,[1] which have held a lot of scientists' interests in the last 40 years.[2−6] In some cases, surface geometry plays an important role on the criteria of PE adsorption[7−10] since it can greatly affect the conformation of the PE chains. In this paper, we focus on the cylindric case, which is motivated by the facts that many stiff macromolecules have rodlike appearances.[11,12] A typical case is the tobacco mosaic virus (TMV),[13] which is an RNA virus and is ∼300 nm in length and ∼18 nm in diameter (thus having a cylindrical geometry).

Although a lot of progress has been made in the study PE of adsorption by charged surfaces, the understanding of PE adsorption is still unsatisfactory; for example, the conformations of PE chains in the adsorbed layer are unclear. The main reason is that there are many parameters, which can all govern the properties of the PE adsorption. These parameters include the molecular weight, the charge distribution and the charge fraction of PE chain, the persistent length, the surface geometry, and the density of surface charges. These systems usually include three interactions, which are the PE chain connectivity, the long-range electrostatic interaction between charges, and the short-range non-Coulombic interaction. Here, the short-range interaction includes the interaction between polymer monomers and solvent molecules (described by Flory−Huggins parameter, χ) and van der Waals interaction between surfaces and PE. The coexistence of these three interactions makes it very difficult to investigate the PE adsorption. Moreover, the salt makes the adsorption process more complicated. It is due to the fact that the salt ions can screen the Coulombic interaction between the charges and can also change the charge distribution and the persistent length of PE chains that leads to the conformational changing of PE. Furthermore, the salt ion and counterion entropies have to be taken into account. All the factors above lag the theoretical treatment of PE adsorption behind the neutral polymer adsorption.

Also, the adsorption−depletion transition is an interesting aspect in the PE adsorption.[6,14−16] Correspondingly, it has already attracted many theoretical, computer simulation, and experimental treatments. A main task is to investigate the scale law between the transition phenomenon and the parameters mentioned above. Plenty of theoretical treatments are based on a single chain model of adsorption. Odijk[17] first performed the binding of a long flexible PE chain to a rodlike oppositely charged macromolecule, ignoring the interactions between the charged monomers and using a Wentzel−Kramers−Brillouin approximation. For the same single chain case, Wiegel[18] theoretically investigated the PE adsorption onto a plane and first showed that a phase transition would occur at a critical value of the adsorption energy, which separates the adsorbed and desorbed states. Late, Muthukumar et al.[7,8] used a combination of variational calculation and the ground-state dominance to study the critical criteria for PE adsorption onto charged planar, cylindrical and spherical surfaces, in which they showed the scaling laws of the critical quantities at the adsorption-depletion transition point, including the density of surface charge, the charges on polymer, Debye screening length, and temperature. Recently, Winkler and Cherstvy[15,16,19] analytically investigated the critical adsorption of a PE chain onto a spherical surface by substituting the Hulthén potential for the Debye−Hückel potential. Their results showed the existence of adsorption−depletion phase-transition-like phenomenon and also gave the scaling laws of critical quantities. Besides the theoretical treatments, Monte Carlo simulations have also been used to study the adsorption of the PE chain onto charged surface. Wallin and Linse[20−22] studied a spherical micelle−polyelectrolyte complex and mainly focused on the effects of the chain flexibility, the charge fraction of PE chain, and the tail length of surfactant on the critical aggregation concentration (CAC) of the micelles. Kong and Muthukumar[23] validated their variational calculation[7,8] by Monte Carlo simulation and obtained a good agreement with their own

* Corresponding author. E-mail: yandd@iccas.ac.cn
[†] Beijing National Laboratory Molecular Sciences (BNLMS), Joint Laboratory of Polymer Science and Materials, Institute of Chemistry, Chinese Academy of Sciences.
[‡] Department of Physics and Astronomy, McMaster University.

10.1021/ma8003482 CCC: $40.75
Published on Web 06/18/2008

theoretical predictions in planar and spherical cases. Similarly, Chodanowski and Stoll[24] investigated a spherical particle−polyelectrolyte complex in which the effects of particle size and ionic concentration on the adsorption−depletion transition have been investigated.

Contrary to the single-chain adsorption, there are fewer theoretical treatments on the critical adsorption in the multichain case. The typical works were carried out by Andelman and Netz et al.[6,14,25,26] They presented the solutions of linearized mean-field equations and showed the scaling law of the salt concentration, C^*_{salt}, the PE chain charge fraction, p, and the density of surface charge, σ, at the adsorption−depletion transition point in the planar surface case, i.e., $C^*_{salt} \sim (\sigma p)^{2/3}$. Haronska et al.[27] assumed that the electrostatic interaction for charges is the Debye−Hückel potential and used self-consistent variational calculation to study the adsorption of PEs onto spherical surface. Meanwhile, lots of experimental results for the critical adsorption onto different surfaces have also been reported.[9,10,28–30] Dubin et al. experimentally showed that the surface curvature do have effects on the criteria of the critical adsorption[9] and gave the scaling index of the critical density of surface charge against the Debye−Hückel parameter, i.e., $\sigma \sim \kappa^b$. For planar, cylindric, and spherical surfaces, the values of b equated to 2.2−3.0, 2.0−2.5, and 1.4, respectively.[10]

The adsorption of flexible polyelectrolytes onto different geometrical charged surfaces can be described well at a quantitative level by self-consistent field theory (SCFT). Van der Schee and Lyklema[31] first extended the lattice SCFT developed by Scheutjens and Fleer[32,33] for neutral polymers to deal with the adsorption of polyelectrolytes. Shi[34] and Wang[35] have independently derived the general formalism of the continuum SCFT of inhomogeneous multicomponent polyelectrolytes systems. We extend their continuum SCFT to the adsorption of flexible polyelectrolytes onto uniformly oppositely charged cylinders, in which the Hamiltonian of the system contains the chain connectivity in the standard Wiener form,[36] the electrostatic interactions between charges (without the usual Debye−Hückel potential approximation), and the short-range van der Waals interactions between the monomers and solvent molecules.

In this paper, we will use the continuum SCFT to study the critical adsorption of the flexible polyelectrolytes onto a cylinder with opposite charges. We will present the simple scaling expressions for the critical quantities at the adsorption−depletion transition point, which are the density of surface charge, the charge fraction of PE chain and the critical concentration of salt for different surface curvatures. In particular, we will find the critical point around which the curvature loses its effect on the scaling expressions. Also, a critical line for the dependence of the critical radius on the salt concentration, which separates the adsorbed and desorbed states, will be found. The theoretical model and numerical method are provided in section II. Results and discussions are presented in section III. Conclusions are summarized in section IV.

II. Theoretical Framework

In this paper, we consider such a system which contains a positively charged cylindrical surface, flexible charged homopolymers with N monomers each, neutral solvent and the small ions, as shown in Figure 1. The small ions come from the PE chains, charged surface counterions and the dissolved salt. Also, we assume that all the small ions are identical and carry the same type of charge which is denoted by ± for cations and anions, respectively. We assume that there are n_P PE chains, n_s solvent molecules, and $n_\pm$ cations and anions, respectively, in a finite volume V. The Kuhn statistical length of the PE chain is a. For simplicity, the bulk density of polymer monomers and solvent molecules are both ρ_0. Also, we ignore the volume of small ions. Integral variables of ν_P, ν_+, and ν_- are the valence numbers (in units of charge e) carried by PE monomers, cations and anions, respectively. We assume that each PE chain is negatively charged and the charge is smeared along the chain with a charge fraction, p. As the cylinder is long enough, and hence the electrostatic field has cylindrical symmetry, we can only consider the variations along the radial direction of the adsorbing surface. We take the center of the cylinder as $r = 0$. The system is in contact with a bulk solution at $r = L$, where L is the distance from the system center to the boundary of bulk phase, as shown in Figure 1.

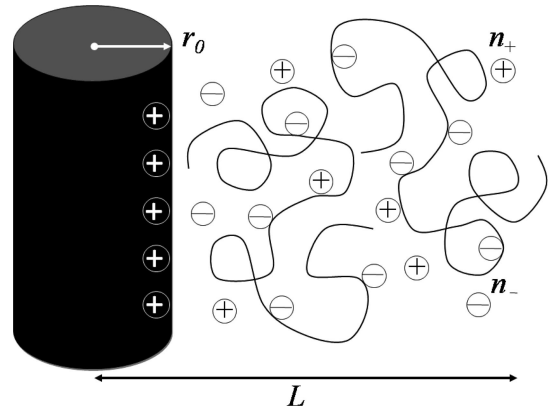

Figure 1. System consisting of a positively charged cylinder surrounded by negatively charged polyelectrolytes with neutralizing counterions and the salt ions in solution. The system contacts with a bulk solution at $r = L$, where L is the distance from the axes of cylinder to the boundary of bulk phase.

We use the bulk density ρ_0 to normalize the polymer monomer density, $\rho_P(r)$, the molecular density of the solvents, $\rho_s(r)$, and the number densities of small ions, $\rho_\pm(r)$, which lead to the dimensionless volume fractions, $\phi_j(r)$, or $\phi_j(r) = \rho_j(r)/\rho_0$ with j = P, s, and ±. In the following section, we will use the convention that the index j runs over all the species of P, s, and ±. We assume that the system is locally incompressible, and hence

$$\varphi_P(r) + \varphi_s(r) = 1 \tag{1}$$

The number of molecules in the volume can also be expressed in terms of the average volume fractions $\phi^{--}_j \equiv (1/L)\int_{r_0}^{L} \mathrm{d}r\, \phi_j(r) = n_j Z_j/\rho_0 V$, where $Z_P = N$ and $Z_s = Z_\pm = 1$. We define the electrostatic potential $\varphi(r)$ in units of k_BT/e to make it dimensionless, where k_B is the Boltzmann constant and T is the temperature. Finally, the volume fraction of the total charged molecules is given by $\phi_e(r) = \nu_P p\phi_P(r) + \nu_+\phi_+(r) + \nu_-\phi_-(r)$, which is also normalized by ρ_0. With the above descriptions, we can write the free energy functional in the form[34]

$$\frac{F[\rho k_BT, \phi(r)]}{\rho_0} = \int \mathrm{d}^3r\left[\sum_j \mu_j\varphi_j(r) + \chi_{Ps}\varphi_P(r)\varphi_s(r)\right] - \int \mathrm{d}^3r\left[\sum_j \omega_j(r)\varphi_j(r) + e\omega_e(r)\varphi_e(r)\right] - \sum_j \frac{\bar{\varphi}_j V}{Z_j}\ln\left(\frac{Q_j}{\bar{\varphi}_j}\right) + \int \mathrm{d}^3r\left[\varphi_e(r)\phi(r) - \frac{a^2}{2\tau}|\nabla\phi(r)|^2\right] \tag{2}$$

where μ_j and χ_{Ps} are defined in ref . The parameter τ is defined by

$$\tau = 4\pi\rho_0 a^2 \frac{e^2}{\varepsilon k_BT} \equiv 4\pi\rho_0 a^2 l_B \tag{3}$$

where $l_B = e^2/\varepsilon k_BT$ is the Bjerrum length; ε is the dielectric constant, which is approximately a constant in the whole space

of the system. We take the bulk density $\rho_0 = a^{-3}$ and the average Kuhn length $a = 0.5$ nm. For aqueous solutions at room temperature, $l_B \approx 0.7$ nm, $\tau^{-1} = 0.057$. $\omega_j(r)$ are the auxiliary fields which couple with the volume fractions $\phi_j(r)$, and $\omega_e(r)$ is the auxiliary field for the charge density. Q_j are the single molecular partition functions defined by

$$Q_P = \frac{1}{L}\int_{r_0}^{L} dr\, q(r,N)$$

$$Q_s = \frac{1}{L}\int_{r_0}^{L} dr \exp[-\omega_s(r)]$$

$$Q_\pm = \frac{1}{L}\int_{r_0}^{L} dr \exp[-\nu_\pm\phi(r)] \quad (4)$$

The propagator $q(r, t)$ corresponds to the probability of finding the end-monomer of a polyelectrolyte of length t at r, which is the solution of the modified diffusion equation

$$\frac{\partial q(r,t)}{\partial t} = \frac{1}{6r}\frac{d}{dr}\left[r\frac{dq(r,t)}{dr}\right] - [\omega_P(r) + p\nu_P\phi(r)]q(r,t) \quad (5)$$

with the initial condition $q(r, t = 0) = 1$, where $t \in [0, N]$ is a variable along the chain contour.

The detailed deriving of the free energy has been presented in refs[34] and.[35] This free energy is too complicated to evaluate directly, and we use the saddle-point approximation to deal with the integrand. Thus, we obtain the following set of self-consistent field equations

$$\varphi_P(r) = \frac{\bar{\varphi}_P}{Q_P N}\int_0^N dt\, q(r,t)q(r,N-t) \quad (6)$$

$$\varphi_s(r) = \frac{\bar{\varphi}_s}{Q_s}\exp[-\omega_s(r)] \quad (7)$$

$$\varphi_\pm(r) = \frac{\bar{\varphi}_\pm}{Q_\pm}\exp[-\nu_\pm\phi(r)] \quad (8)$$

$$\omega_s(r) = \omega_P(r) + \chi_{Ps}[2\varphi_P(r) - 1] \quad (9)$$

$$\frac{1}{r}\frac{d}{dr}\left[r\frac{d\phi(r)}{dr}\right] = -\tau\left\{\nu_P p\varphi_P(r) + \frac{\nu_+\bar{\varphi}_+}{Q_+}\exp[-\nu_+\phi(r)] + \frac{\nu_-\bar{\varphi}_-}{Q_-}\exp[-\nu_-\phi(r)]\right\} \quad (10)$$

Finally, the incompressibility and the charge neutrality constraints in the system give

$$\bar{\varphi}_P + \bar{\varphi}_s = 1 \quad (11)$$

$$\nu_P p\bar{\varphi}_P + \nu_+\bar{\varphi}_+ + \nu_-\bar{\varphi}_- + \sigma = 0 \quad (12)$$

where the dimensionless area density of surface charge is given by $\sigma \equiv \sigma_0/a^{-2}$, in which σ_0 is the area density of surface charges.

We take the boundary conditions of the modified diffusion equation, eq 5, and the Poisson−Boltzmann equation, eq 10, as follows. At $r = r_0$, the boundary condition for the PE propagators is $q(r = r_0, t) = 0$, corresponding to a nonadsorbing surface. Meanwhile, we take the density of surface charge as a constant, which gives $d\varphi/dr|_{r=r_0} = -4\pi\sigma l_B/a^2$. As we preassumed that all density functions of the system are invariant at $r = L$, we use $dq/dr|_{r=L} = 0$ and $d\varphi/dr|_{r=L} = 0$ as the other boundary conditions. The volume fractions of polymer monomer and salt in the bulk solution are given by $\phi_{P,b}$ and C_{salt}, respectively. In the bulk solution, the system locally charges neutrality, indicating that the electrostatic potential equates to zero, or, $\varphi(r) = 0$. The concentration of the cations, anions, salt and polymer monomers in the bulk solution have the following relations

$$\frac{\nu_+\bar{\varphi}_+}{Q_+} = \nu_+ C_{salt} - \nu_P p\varphi_{P,b}$$

$$\frac{\nu_-\bar{\varphi}_-}{Q_-} = \nu_- C_{salt} \quad (13)$$

where $\phi_{P,b}$ and C_{salt} are the dimensionless concentrations of polymer monomer and salt in the bulk solution, respectively. We assume that one salt molecule generates one cation. Furthermore, to make sure the chemical potential in the both sides of $r = L$ continuous, we take

$$\varphi_P(L) = \varphi_{P,b} \quad (14)$$

Since the SCFT equations are highly nonlinear, we have to discretize the space and solve these equations numerically in the real space. The numerical method follows Wang's work,[37] in which the combination of Broyden's method and a globally convergent strategy[38] is used to solve the set of nonlinear equations. The Crank−Nicolson scheme is used to solve the modified diffusion equation. The spatial domain $[r_0, L]$ is discretized into n grids. The number of n is on the order of 10^3-10^4 to make sure that the numerical results of the electrolyte potential in the bulk solution is on the order of 10^{-10}. To indicate adsorption and depletion, we define the surface excess, Γ, as the total amount of monomers taking part in the adsorption layer per unit length on the cylinder, or, $\Gamma = \int_{r_0}^{L} r[\phi_P(r) - \phi_{P,b}]\, dr$. Polymers are depleted from the surface when $\Gamma < 0$ and adsorbed by the surface when $\Gamma > 0$. The place where $\Gamma = 0$ corresponds to an adsorption−depletion transition.

III. Results and Discussions

Throughout this paper, the degree of polymerization of the PE chains is $N = 200$. The Kuhn statistical length is $a = 0.5$ nm and the gyration radius is $R_g = 5.8a$. All lengths are scaled by a; meanwhile, all the number densities of polymer monomers, solvents, and small ions are normalized by the bulk density, $\rho_0 = a^{-3}$. According to these conventions, $\phi_{P,b} = 1.25 \times 10^{-4}$ corresponds to the bulk molar density of polymer monomer $\rho_P = \phi_{P,b}\rho_0/N_A = 1.66$ mM, $C_{salt} = 0.006$ corresponds to the bulk molar concentration of salt $C^M_{salt} = C_{salt}\rho_0/N_A = 80$ mM. Here, N_A is Avogadro's number. Also, $\sigma = 0.025$ corresponds to the density of surface charge $\sigma_0 = \sigma(1/a^2) = 10^{-3}$ Å^{-2}. Hereafter, we only consider the monovalent systems and take $\nu_P = \nu_- = -\nu_+ = -1$.

An important scaling expression is the relationship between the charge fraction of PE chain, p, the density of surface charge on the cylinder, σ, and the salt concentration at the adsorption-depletion transition point, C^*_{salt}, or

$$C^*_{salt} \sim p^{\alpha(r_0)}\sigma^{\beta(r_0)} \quad (15)$$

which can well describe the behavior of critical adsorption of PEs. The validity of the this relation has been demonstrated experimentally for many systems of polyelectrolytes and oppositely charged micelles or dendrimers.[10,28,29] Here, we first use the SCFT to obtain the scale relationship between C^*_{salt} and σ in the small surface curvature. We select the value of σ_0 from 4×10^{-5} Å^{-2} to 2×10^{-3} Å^{-2} to make sure the value of σ is wide enough to demonstrate the existence of the scaling relationship. The numerical result is shown in a log−log manner in Figure 2, which describes well the adsorption−depletion transition phenomena. An approximate $^2/_3$ power law of C^*_{salt} with σ, or $C^*_{salt} \sim \sigma^{2/3}$, is found, which demonstrates the validity of the scaling relationship. Different from the plane case, the surface curvature also plays an important role in determining the final form of eq 15. In the following section, we investigate different surface curvatures by changing the cylinder radius r_0

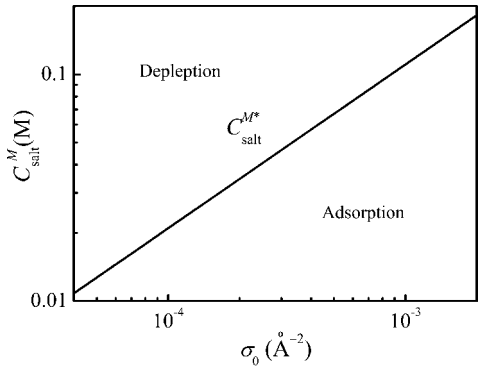

Figure 2. Log−log scaled diagram of adsorption−depletion crossover for wide values of σ from 4×10^{-5} to 2×10^{-3} at small surface curvature ($r_0 = 100R_g$). Numerical result gives a good scaling expression, which is approximately $C^*_{salt} \sim \sigma^{2/3}$.

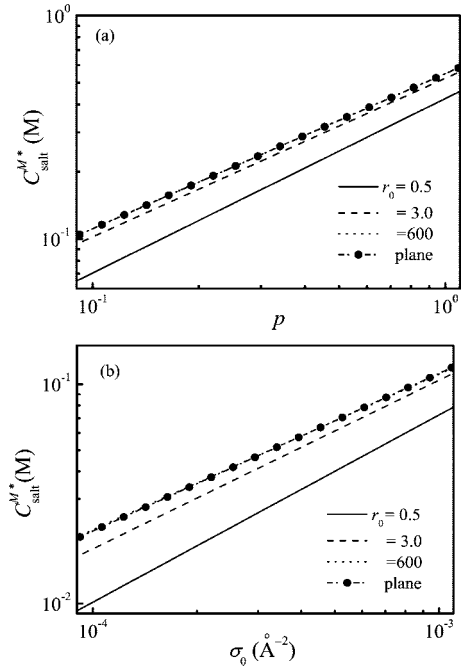

Figure 3. Adsorption-depletion crossover diagram for both planar and cylindrical surface. (a) The log−log scale of C^*_{salt} and p for fixed $\sigma = 0.025$. The scale exponents from the linear fitting are 0.78 ± 0.02, 0.71 ± 0.03, and 0.69 ± 0.02 for $r_0 = 0.5$, 3, and 600, respectively. (b) The log−log scale of C^*_{salt} and σ for fixed $p = 0.1$. The scale exponents from the linear fitting are 0.86 ± 0.03, 0.77 ± 0.02, and 0.71 ± 0.02 for $r_0 = 0.5$, 3, and 600, respectively.

from $r_0 = 0.5$ ($\sim 0.1R_g$) to $r_0 = 600$ ($\sim 120R_g$) to see how the exponents α and β change with r_0.

Figure 3 is the direct evidence of the effects of surface curvature on the scaling expression in eq 15. Figure 3a shows the log−log phase diagram of C^*_{salt} and p for fixed σ, including both planar and cylindrical surface results. We independently investigated the planar case by SCFT. The least-mean-square fit lines of numerical date separate adsorbed and desorbed states. Their slopes, or the values of α, are 0.78 ± 0.02, 0.71 ± 0.03, and 0.69 ± 0.02 for $r_0 = 0.5$, 3, and 600, respectively. In particular, the fitting line for small curvature ($r_0 = 600$) completely overlaps the result of the planar surface. Meanwhile, the log−log phase diagram of C^*_{salt} and σ for fixed p is presented in Figure 3b. The adsorption−depletion transition is well described by the least-mean-square fitting lines and the values of β are 0.86 ± 0.03, 0.77 ± 0.02, and 0.71 ± 0.02 for $r_0 = 0.5$, 3, and 600, respectively. Again, the result of the small curvature recovers the result of the planar case. From parts a and b of Figure 3, we find that the exponential values of α and β decrease as r_0 increases, which means that there are different scaling forms of the critical quantities for different surface curvatures. The exponential values at the large cylinder radius ($r_0 = 600$) gives an approximate $^2/_3$ power law of C^*_{salt} against both p and σ, or $C^*_{salt} \sim (p\sigma)^{2/3}$. The result is in agreement with the planar surface case obtained by others[8,14] and ourselves. Contrarily, different α and β values appear at the small cylinder radius ($r_0 = 0.5$), or $C^*_{salt} \sim p^{0.78}\sigma^{0.86}$. We change the scaling of C^*_{salt} against σ to the scaling of σ against the inverse Debye screening length κ, and obtain $\sigma \sim \kappa^{2.3}$, which yields a good agreement with the experimental data.[10] By now, we have found that the surface curvature does have effects on the scaling expression, eq 15, which means that we have different scaling forms for different surface curvatures. In the following section, however, more numerical results show that a crossover point exists in the whole curvature dimension. As r_0 becomes larger than it, the curvature will lose its effects on the scaling expression.

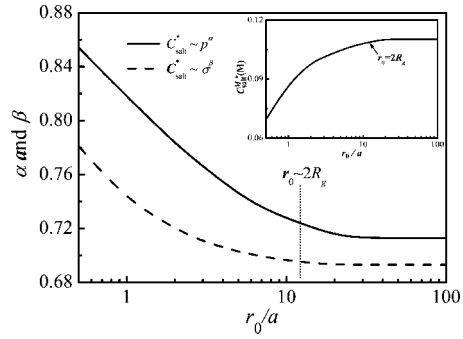

Figure 4. Effect of surface curvature on the scaling law. α and β are obtained for fixed $\sigma = 0.025$ and for fixed $p = 0.1$, respectively. The scale exponents decrease as r_0 increases when $r_0 < 2R_g$. As r_0 goes larger than $2R_g$, the scale exponents nearly do not change with r_0 and approach the fixed values of the planar surface, i.e., 2/3. The insert is the r_0 dependence of C^*_{salt}. C^*_{salt} increases as r_0 increases and quickly converges to the result of the planar surface as r_0 becomes larger than $2R_g$.

Figure 4 shows the dependence of α and β on the surface curvature. Also, it shows the dependence of the critical salt concentration C^*_{salt} on the surface curvature. We change the surface curvature by increasing the cylinder radius from 0.5 to 100. We obtain the scaling expressions of C^*_{salt} with p, as well as C^*_{salt} with σ respectively. The results show that both α and β decrease as r_0 increases, on the contrary, C^*_{salt} increases as r_0 increases. However, when the radius goes larger than $2R_g$, α, β, and C^*_{salt} nearly do not change with the radius and quickly converge to the values of the planar case. This is not a sharp transition but a crossover. Here, we define the point $r_0 \sim 2R_g$ as the crossover point which divides the curvature dimension into two regimes, or, cylindrical regime for $r_0 < 2R_g$ and planar regime for $r_0 > 2R_g$. It is worth remembering that this crossover point is universal in the cylindrical system, because it is independent of other parameters.

The main result can be found in Figure 4, where we obtain two regimes based on the effects of the surface curvature on the critical adsorption of PEs. One is the planar regime with $r_0 > 2R_g$, while the other is the cylindrical regime with $r_0 < 2R_g$. The crossover point is around $r_0 \sim 2R_g$ and is universal in all cylindrical systems. In the planar regime, the scaling expression does not change with r_0 and has almost the same form as the results of planar surface, i.e., $C^*_{salt} \sim (p\sigma)^{2/3}$. Moreover, the critical quantities are also invariable with r_0. It means that the surface curvature loses its effect on the criteria of the critical adsorption of PEs in this regime. In the cylindrical regime, however, as r_0 decreases the values of α and β increase, and C^*_{salt} decreases.

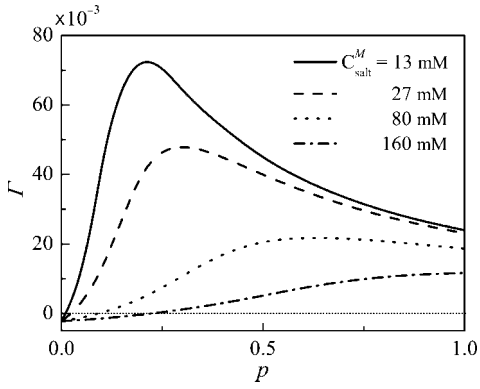

Figure 5. Γ dependence on p for several C_{salt}^{M} of 13 mM (solid line), 27 mM (dashed line), 80 mM (dotted line), and 160 mM (dashed-dotted line) at $\sigma = 0.025$.

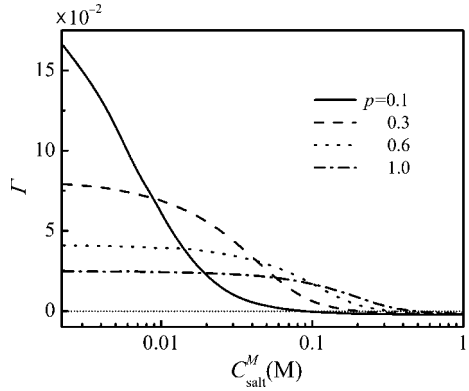

Figure 6. Γ dependence on C_{salt}^{M} for several p of 0.1 (solid line), 0.3 (dashed line), 0.6 (dots line), and 1.0 (dashed-dotted line) at $\sigma = 0.025$.

The scaling expression changes with r_0 rather than the r_0 independent exponents in planar regime. For example, at small radius $r_0 = 0.5$, $C_{salt}^{*} \sim p^{0.78}\sigma^{0.86}$. There are two reasons for the existence of the two different regimes in this system. One reason is that the PE chains have larger entropy loss when they are adsorbed on the surface with larger curvature (small r_0). The other reason is that the electrostatic field distribution along the radial direction is different for different radii. These differences become small when the size of cylinder increases comparable to the size of PE. The numerical results show that when r_0 goes larger than $2R_g$, the two factors above are invariable with r_0 and have the same effect on critical adsorption as that in the planar surface case. This means that the surface curvature loses its effect on the critical criteria of PE adsorption in this regime and the critical point is $r_0 \sim 2R_g$.

Although the surface curvature has effect on the scaling expression of the critical quantities, it weakly affects the surface excess, Γ. In Figure 5 the dependence of Γ on p is shown for different salt concentrations C_{salt} while the system is in the cylindrical regime for $r_0 = 1.0$. We find that there is a peak in $\Gamma(p)$ in the adsorption regime ($\Gamma > 0$), and the peak decreases and shifts to a higher value of p as C_{salt} increases, because when C_{salt} increases the increasing screening reduces the electrostatic adsorption, and hence a stronger electrostatic attractive interaction is needed. A depletion to adsorption transition can be found as p increases. Figure 6 presents the effect of C_{salt} on Γ for different p while the system is also in the cylindrical regime with $r_0 = 1.0$. As C_{salt} increases, Γ monotonously decreases and $\Gamma > 0$ crosses over to $\Gamma < 0$, signaling the adsorption−depletion transition. The behaviors in Figure 5 and Figure 6 are quite similar to the results in the planar adsorption system,[6,39,40] which indicates that surface curvature has less effect on Γ.

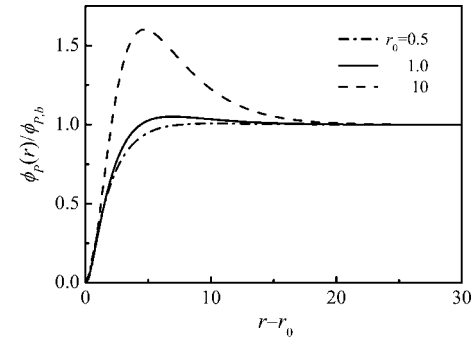

Figure 7. Comparison of the radial normalized monomer density distribution at $\sigma = 10^{-3}$ e Å^{-2} and $C_{salt} = 860$ mM for different radii of $r_0 = 0.5$, (dashed-dotted line), 1.0 (solid line), and 10 (dashed line), where $r_0 = 1.0$ indicates the adsorption−depletion transition according to the value of the surface excess.

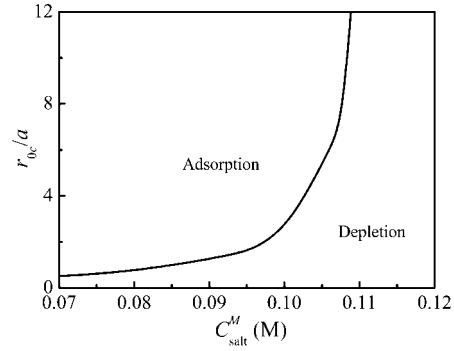

Figure 8. The C_{salt}^{M} dependence of the critical radius. The critical line separates the adsorption regime from the depletion regime for $\sigma = 0.025$ and $p = 0.1$.

Above, we have studied the combination effects of σ, C_{salt}, p, and r_0 on PE critical adsorption. Hereafter, we want to fix all the parameters but the cylindrical radius r_0 and to see what will happen in this system. Fixing $\sigma = 0.025$, $C_{salt} = 0.0065$, and $p = 0.1$, we studied the effect of changing r_0 on PE critical adsorption. Figure 7 shows the radial monomer density $\phi_P(r)$ distribution for different radii, where $\phi_P(r)$ is normalized by $\phi_{P,b}$. $\phi_P(r)$ increases as r_0 variates from 0.5 to 10, while the peak shifts to larger radial distances. It occurs in the limit $r \to \infty$ for small radius $r_0 = 0.5$, which means that depletion rather than adsorption happens. The results show that the adsorption−depletion transition can be tuned only by r_0. The reason is that with a constant surface charge density, decreasing r_0 reduces the total number of charges on the surface, and hence reduces the electrostatic energy between the surface and PE polymers. If all the parameters are fixed except r_0, the adsorption-depletion transition at a critical radius $r_{0,c}$ will happen. Figure 8 shows the critical $r_{0,c}$ for different C_{salt}. The left side corresponds to the adsorption regime while the right side corresponds to the depletion regime. The critical line in the cylindrical system is quite similar to that in a single chain adsorption onto an oppositely charged spherical system.[8,19,23]

Finally, we discuss the limitation of the present model. As the SCFT is at mean-field level, in the present model we did not consider the lateral correlations and fluctuations, which can alter the adsorption behavior.[5,6] Another approximation is that we did not consider the non-Coulombic attractive interaction between the surface and the PE chains. However, if this interaction is comparable to the electrostatic interaction, it can also overcome the entropy loss and have strong effects on the adsorption. Also, omitting the volume of the small ions is also a limitation of the present work. These ions compete with polymers for surface adsorption and do effect on the

adsorption−depletion transition. Moreover, the polyelectrolytes may undergo a so-called Manning counterion condensation at a high charge density. In the present work, we only consider the weakly charged monovalent polyelectrolyte system in which the Manning condensation is unnecessary to be considered if $l_B\tau < 1$.[6] In the present system, we take the typical values of $l_B = 0.7$ nm. Using $\tau = p/a$, we find that for the values of charge fractions $p < 0.7$, we have $l_B\tau < 1$. In other words, the calculation in the present work is only valid for $p < 0.7$ if we do not consider the Manning counterion condensation. In fact, in the nature strongly charged and rigid polymer are more universal rather than weakly charged and flexible PE chains. Thus, a different model, beyond a Gaussian chain model, is needed.[12] This could be the topic for our future work.

IV. Conclusions

Within the continuum SCFT including multichain interactions, we studied the adsorption of flexible polyelectrolytes onto uniformly oppositely charged cylindrical surface. We show that the adsorption−depletion phase-transition-like phenomenon exits in the cylindrical case. Furthermore, the numerical results show that this phenomenon can be tuned not only by the salt and the chain charge fraction but also by the cylindrical radius, which means that the surface curvature plays an important role in the critical adsorption of PEs. The main discussions focus on the effect of surface curvature on the critical adsorption of PEs. On the basis of the scale expression, we divide the whole curvature dimension into two regimes, namely, a planar regime for $r_0 > 2R_g$ and a cylindrical regime for $r_0 < 2R_g$. Between the two regimes there is not a sharp transition but a crossover. Numerically, the crossover point is around $r_0 \sim 2R_g$, which is independent of other parameters. In the cylindrical regime, the indexes of α and β in the scaling expression eq 15 continuously increase as r_0 decreases. For the small radius $r_0 = 0.5$, the scaling expression eq 15 becomes $C^*_{salt} \sim p^{0.78}\sigma^{0.86}$, in which the relation between the surface charge density and the salt concentration $\sigma^{0.86} \sim C^*_{salt}$ is in agreement with the experimental results; In the planar regime, the scaling expression eq 15 is independent of the surface curvature and has the form, approximately, of $C^*_{salt} \sim (p\sigma)^{2/3}$, which is in agreement with the result by ground-state dominance approximation for the planar case. We also studied the dependence of the surface success Γ on the salt concentration C_{salt} and chain charge fraction p in the cylindrical regime. The results show that this dependence is less affected by the surface curvature and has a similar behavior to the planar adsorption case. Moreover, we also find an universal critical line for the cylindrical radius as a function of the salt concentration, which separates adsorbed and desorbed states. The critical line is similar to the adsorption of a single chain onto an oppositely charged spherical surface.

Acknowledgment. We would like to acknowledge helpful discussions with Tongchuan Suo and Lijian Qu. This work is supported by the National Natural Science Foundation of China, Grants NSFC 20575085 and NSFC 20490220, and also a grant from Chinese Academy of Sciences, Grant KJCX2-YW-206. A.-C.S. acknowledges support from the Natural Science and Engineering Research Council (NSERC) of Canada.

References and Notes

(1) Dautzenberg, H.; Jaeger, W.; Kotz, J.; Philipp, B.; Seidel, Ch.; Stscherbina, D. *Polyelectrolytes: Formation, Characterization and Application*; Hanser Gardner: Munich, Germany, 1994.
(2) Kawaaguchi, M.; Takahashi, A. *Adv. Colloid Interface Sci.* **1992**, *37*, 219.
(3) Fleer, G. J.; Cohen Stuart, M. A.; Scheutjens, J. M. H. M.; Gasgove, T.; Vincent, B. *Polymer at interfaces*; Chapman and Hall: London, 1993.
(4) Bajpai, A. K. *Prog. Polym. Sci.* **1997**, *22*, 523.
(5) Dobrynin, A. V.; Deshkovski, A.; Rubinstein, M. *Macromolecules* **2001**, *34*, 3421.
(6) Netz, R. R.; Andelman, D. *Phys. Rep.* **2003**, *380*, 1.
(7) Muthukumar, M. J. *Chem. Phys.* **1987**, *86*, 7230.
(8) van Goeler, F.; Muthukumar, M. J. *Chem. Phys.* **1994**, *100*, 7796.
(9) Yingjie, L.; Dubin, P. L.; Spindler, R.; Tomalia, D. A. *Macromolecules* **1995**, *28*, 8426.
(10) Feng, X. H.; Dubin, P. L.; Zhang, H. W.; Kirton, G. F.; Bahadur, P.; Parotte, J. *Macromolecules* **2001**, *34*, 6373.
(11) Grosberg, A. Yu.; Nguyen, T. T.; Shklovskii, I. *Rev. Mod. Phys.* **2002**, *74*, 329.
(12) Boroudjerdi, H.; Kim, Y.-W.; Naji, A.; Netz, R. R.; Schlagberger, X.; Serr, A. *Phys. Rep.* **2005**, *416*, 129.
(13) Creager, A. N. *The Life of a Virus: Tobacco Mosaic Virus as an Experimental Model, 1930−1965*; University of Chicago Press: Chicago, IL, 2002.
(14) Shafir, Adi.; Andelman, D. J. *Chem. Phys.* **2003**, *119*, 2355.
(15) Winkler, R. G.; Cherstvy, A. G. *Phys. Rev. Lett.* **2006**, *96*, 0066103.
(16) Cherstvy, A. G.; Winkler, R. G. J. *Chem. Phys.* **2006**, *125*, 064904.
(17) Odijk, T. *Macromolecules* **1982**, *13*, 1542.
(18) Wiegel, F. W. *J. Phys. A: Math. Gen.* **1977**, *10*, 299.
(19) Winkler, R. G.; Cherstvy, A. G. *J. Phys. Chem.* **2007**, *111*, 8486.
(20) Wallin, T.; Linse, P. *Langmuir* **1996**, *12*, 305.
(21) Wallin, T.; Linse, P. *J. Phys. Chem.* **1996**, *100*, 17873.
(22) Wallin, T.; Linse, P. *J. Phys. Chem. B* **1997**, *101*, 5506.
(23) Kong, C. Y.; Muthukumar, *J. Chem. Phys.* **1998**, *109*, 1522.
(24) Chodanowski, P.; Stoll, S. J. *Chem. Phys.* **2001**, *115*, 4951.
(25) Netz, R. R.; Joanny, J. F. *Macromolecules* **1999**, *32*, 9013.
(26) Netz, R. R.; Andelman, D. In *Encyclopedia of Electrochemistry*; edited by Urbakh, M., Giladi, E. , Eds.; Wiley-VCH: Weinheim, Germany, 2002; Vol. *1*.
(27) Haronska, P.; Vilgis, T. A.; Grottenmüller, R.; Schmidt, M. *Macromol. Theory Simul.* **1998**, *7*, 241.
(28) Dubin, P. L.; Thé, S. S.; McQuigg, D. W.; Chew, C. H.; Gan, L. M. *Langmuir* **1989**, *5*, 89.
(29) Miura, N.; Dubin, P. L.; Moorefield, C. N.; Newkome, G. R. *Langmuir* **1999**, *15*, 4245.
(30) Yilin, W.; Dubin, P. L.; Huiwen, Z. *Langmuir* **2001**, *17*, 1670.
(31) Van der Schee, H. A.; Lyklema, J. J. *Phys. Chem.* **1984**, *88*, 6661.
(32) Scheutjens, J. M. H. M.; Fleer, G. J. J. *Phys. Chem.* **1979**, *83*, 1619.
(33) Scheutjens, J. M. H. M.; Fleer, G. J. J. *Phys. Chem.* **1980**, *84*, 178.
(34) Shi, A. C.; Noolandi, J. *Macromol. Theory Simul.* **1999**, *8*, 214.
(35) Wang, Q.; Taniguchi, T.; Fredrickson, G. H. *J. Phys. Chem. B* **2004**, *108*, 6733. 2005, 109, 9855.
(36) Doi, M.; Edwards, S. F. *The Theory of Polymer Dynamics*; Oxford Press: New York 1986.
(37) Wang, Q. *Macromolecules* **2005**, *38*, 8911.
(38) Press, W. H.; Teukolsky, S. A.; Vetterling, W. T.; Flannery, B. P. *Numerical Recipes in C: the Art of Scientific Computing*, 2nd ed.; Cambridge University Press: Cambridge, U.K., 2002; Chapter 9.7.
(39) Borukhov, I.; Aandelman, D.; Orland, H. *Macromolecules* **1998**, *31*, 1665.
(40) Borukhov, I.; Aandelman, D.; Orland, H. *Europhys. Lett.* **1995**, *32*, 499.

MA8003482